# Recurrent Bursts via Linear Processes in Turbulent Environments

Geert Brethouwer,[1,*] Philipp Schlatter,[1] Yohann Duguet,[2] Dan S. Henningson,[1] and Arne V. Johansson[1]
[1]Linné FLOW Centre and Swedish e-Science Research Centre, KTH Mechanics, SE-100 44 Stockholm, Sweden
[2]LIMSI-CNRS, UPR 3251, Université Paris-Sud, F-91403 Orsay, France
(Received 3 July 2013; published 10 April 2014)

Large-scale instabilities occurring in the presence of small-scale turbulent fluctuations are frequently observed in geophysical or astrophysical contexts but are difficult to reproduce in the laboratory. Using extensive numerical simulations, we report here on intense recurrent bursts of turbulence in plane Poiseuille flow rotating about a spanwise axis. A simple model based on the linear instability of the mean flow can predict the structure and time scale of the nearly periodic and self-sustained burst cycles. Poiseuille flow is suggested as a prototype for future studies of low-dimensional dynamics embedded in strongly turbulent environments.

DOI: 10.1103/PhysRevLett.112.144502 PACS numbers: 47.20.-k, 47.27.ed, 47.27.ek, 47.32.Ef

Environments with strong fluctuations frequently display regular or chaotic large-scale dynamics. Well-known astrophysical examples are the reversals of large-scale planetary magnetic fields, which are chaotic for Earth but time periodic for the Sun [1]. Other geophysical and astrophysical manifestations of large-scale instabilities include climate cycles on Earth [2] and solar flares [3]. Random reversals of a large-scale circulation are also found in Rayleigh-Bénard convection [4], and in von Kármán [5] and laboratory fluid dynamo experiments [6].

Recurrent large-scale oscillations or bursts like in tokamak plasmas [7] and accretion disks [8] are important manifestations of large-scale instabilities in the presence of (strong) fluctuations. Because of their complexity and the very different scales involved, bursting phenomena are frequently investigated in the laboratory using simplified flow prototypes that capture the essential features of these large-scale instabilities. Such prototypes are usually based on simple geometries while the dominant mechanisms under study are preserved, e.g., the interaction between shear and rotation, convection or Lorentz forces. A bifurcation from full turbulence to an intermittently bursting turbulent regime was recently observed in large-gap Taylor-Couette flows with counterrotating cylinders [9]. The bifurcation was found to coincide with the optimal torque parameters. A striking feature of the large-scale instabilities in the aforementioned systems is their apparent low dimensionality, despite the fact that they happen in environments with intrinsic strong (usually turbulent) fluctuations. Nevertheless, the fundamental cause of these large-scale dynamics is not always understood and it is often arduous to derive elementary models from first principles.

In this Letter, we describe the occurrence of violent *time-periodic* bursts in an as yet unexplored parameter range of turbulent plane rotating Poiseuille flow (RPF), seen as a canonical example of interaction between shear and rotation. The flow develops a large-scale linear instability under the influence of rotation even though it is strongly turbulent. This linear instability is followed by a distinct sequence of processes leading to a self-sustaining cycle of recurrent bursts of turbulence. We demonstrate that the linear instability of the mean flow captures the essential features of the recurrent bursts. We thus argue that RPF is a relevant example of low-dimensional dynamics embedded in a high-dimensional system with strong fluctuations, and can serve as a new prototype for future studies of large-scale dynamics.

The RPF case considered here is a pressure-driven plane channel flow between two smooth parallel flat walls subject to a global rotation about the spanwise axis orthogonal to the mean flow and parallel to the walls; see Fig. 1 for a schematic. The velocity field $\mathbf{u}$ is governed by the incompressible Navier-Stokes equations in the rotating frame

$$\frac{\partial \mathbf{u}}{\partial t} + \mathbf{u}\cdot\nabla\mathbf{u} = -\nabla p + \frac{1}{R}\nabla^2\mathbf{u} - \Omega(\mathbf{e_z}\times\mathbf{u}), \quad (1)$$

$$\nabla\cdot\mathbf{u} = 0, \quad (2)$$

where $\mathbf{e_z}$ is the unit vector in the spanwise $z$ direction and $p$ is a modified pressure including the (dynamically inactive) centrifugal force [10]. Streamwise and wall-normal coordinates are denoted by $x$ and $y$, respectively. The equations are nondimensionalized by the channel half gap $h$ and bulk velocity $\mathcal{U}$ (an average in the $y$ direction), which is kept constant in time, giving $R = \mathcal{U}h/\nu$ and $\Omega = 2\Omega^f h/\mathcal{U}$, where

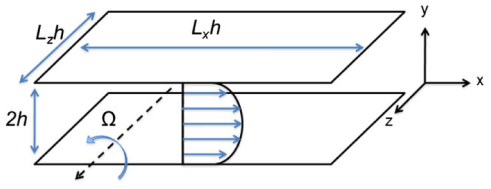


FIG. 1 (color online). Schematic of RPF geometry.

 

$\nu$ is the kinematic viscosity, $\Omega^f$ is the imposed dimensional global rotation rate, and time $t$ is nondimensionalized with $h/\mathcal{U}$.

The governing equations are rewritten in the divergence-free velocity-vorticity formulation and projected numerically on a Fourier-Chebyshev spectral expansion. Time is advanced using a standard semi-implicit Crank-Nicolson and Runge-Kutta scheme [11]. Boundary conditions are periodic in $x$, $z$ and no slip at $y = \pm 1$. The streamwise and spanwise domain size, $8\pi$ and $3\pi$, respectively, are large enough to capture large-scale intermittency and long wavelength instabilities. A resolution of $1152\times217\times864$ spectral collocation points in $x$, $y$, $z$ is used to fully resolve turbulence.

Rotation about the spanwise axis leads to an asymmetric mean velocity profile in three-dimensional turbulent RPF since it amplifies turbulence on the channel side where the vorticity associated with the mean flow $-\mathbf{e_z}dU/dy$ is antiparallel to the rotation vector $\Omega\mathbf{e_z}$, whereas on the other channel side they are parallel and turbulence is damped [12]. Henceforth, we refer to these highly and weaker turbulent channel sides as HTS and WTS, respectively.

RPF at $R = 20\,000$ bifurcates from homogeneous to spatially intermittent turbulence on the WTS and the mean wall shear stress decreases with increasing $\Omega$. At $\Omega = 0.45$ oblique turbulent-laminar bands develop. Similar intermittent patterns have been identified in several transitional flows [13], but in RPF they are confined near the wall, as reported in other shear flows with damping external forces [14]. The second bifurcation from spatially intermittent turbulence to cyclic turbulent bursts takes place slightly below $\Omega = 0.9$.

We focus now on cyclic turbulent bursts in RPF at $R = 20\,000$ and $\Omega = 1.2$. Here $y \lesssim 0.25$ and $y \gtrsim 0.25$ correspond to the HTS and WTS, respectively. Vortical structures seen in Fig. 2 illustrate the vigorous turbulence on the HTS with fluctuations ~5%. Turbulent fluctuations on the WTS are less intense due to the damping effect of rotation yet they are still significant in amplitude. About 200 time units before a turbulent burst occurs, a steadily growing plane wave with streamwise and spanwise wave numbers $\alpha = 2\pi/\lambda_x = 1$ ($\lambda_x$ is the streamwise wavelength) and $\beta = 0$, respectively, and phase speed ≈0.2, appears on the WTS [Fig. 2(a)]. As the wave amplitude becomes large the wave starts to bend owing to a secondary instability akin to $H$-type boundary layer transition [15] producing a typical staggered pattern of Λ-shaped vortices [Figs. 2(b) and 2(c)]. The wave then breaks down into a burst of small-scale turbulence on the WTS while turbulence on the HTS remains unaltered [Fig. 3(a)]. This intense turbulence on the WTS is damped by rotation and decays within 100 time units until the intensity reaches its initial level again [Fig. 2(d)], whereafter the plane wave starts to grow again. This process leads to a self-sustained cycle of intense turbulence bursts with sharp peaks in both turbulent kinetic energy and wall shear stress on the WTS [Fig. 3(b)]. The cycle period of ~1000, being much longer than typical turbulent time scales of ~1, rules out a *direct* forcing by the turbulence fluctuations. The total turbulent kinetic energy grows by ≈80% during a burst, ≈20% of which corresponds to the planar ($\alpha = 1$, $\beta = 0$) wave.

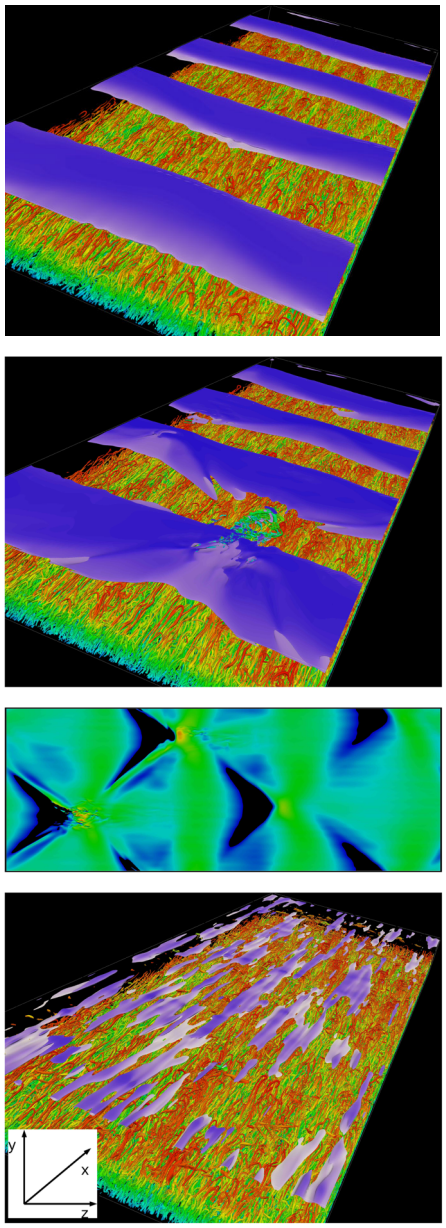


FIG. 2 (color online). Visualizations of the vortical structures on the HTS, with instabilities and turbulent bursts on the WTS at (a) $t = 7233$, (b) $t = 7267$, (d) $t = 7367$. Panel (c) shows the secondary instability at $t = 7267$ in a wall-parallel plane. Flow is from the lower left corner to the upper right corner and the bottom side corresponds to the HTS in (a),(b),(d).

This wave bears similarities with Tollmien-Schlichting (TS) waves produced via a linear instability of laminar Poiseuille flow, albeit there the eigenfunction is symmetric and has a large amplitude on both channel sides. To assess

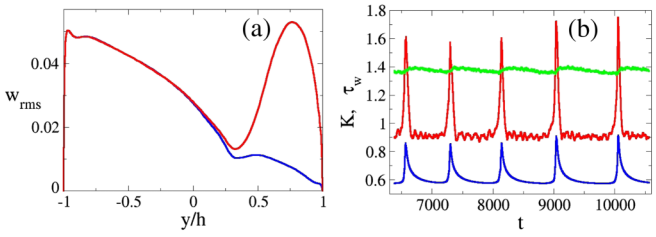


FIG. 3 (color online). (a) Root mean square of the spanwise velocity fluctuations during periods without (blue line, bottom) and with bursts (red line). (b) Time series of the plane averaged wall shear stress on the HTS (green line, top) and WTS (blue line, bottom), and the volume integrated turbulent kinetic energy (red line).

whether the cyclic bursts in RPF are caused by a similar instability, we have carried out a linear stability analysis of a specific base flow. The chosen base flow is incompressible and contains only the streamwise component $U(y)$ of the velocity field spatially averaged in the homogeneous $x$, $z$ directions (the other two components have zero mean). Following standard procedures, the linear equations for the wavelike perturbations $\boldsymbol{u}' = \hat{\boldsymbol{u}}(y)\exp[i(\alpha x + \beta z - \omega t)]$ with real wave numbers $\alpha$, $\beta$ and complex frequency $\omega$ are derived, yielding an eigenvalue problem for $\omega$. Modes with $\beta = 0$, such as the plane wave in Fig. 2, are unaffected by rotation, in contrast to modes with $\beta \neq 0$. We only consider the dominant $\beta = 0$ modes whose evolution, governed by the Orr-Sommerfeld equations, depends on $R$ and the base flow $U(y)$ but not on $\Omega$.

Figure 4(a) shows that this base flow hardly evolves over the period $t = 7680 - 8040$ before the burst, but after the burst at $t \approx 8140$ it changes on the WTS. We infer that the turbulence has a limited *direct* influence on the perturbation since its time and length scale are much smaller. Figure 4(b) shows the growth rate of the most unstable eigenvalue of the $\beta = 0$ modes at various times. Perturbations with $(\alpha \approx 1, \beta = 0)$ have a single unstable eigenvalue prior to the burst at $t \approx 8140$ and are thus linearly unstable, while over a short period after the burst all $\beta = 0$ modes are stable and decay according to linear analysis. The same pattern is found before and after every burst, confirming the robustness of the results. Including a turbulent viscosity in the stability analysis [16] lowers the growth rate by about 10%; yet it does not affect the results significantly, suggesting that turbulence has a limited direct influence despite its intensity. We can thus infer that rotation modifies the mean flow $U(y)$ so that it becomes receptive to a linear instability; nonrotating plane turbulent channel flow has a linearly stable base flow $U(y)$ and does not show large-scale instabilities.

Figure 5(a) shows the exponential growth of the $(\alpha = 1, \beta = 0)$ mode, with a mean growth rate of $\approx 7.5 \times 10^{-3}$ as predicted by the stability analysis, compared to its time evolution extracted from the simulation. The amplitude $u'$ of the mode, corresponding to the plane wave in Fig. 2,

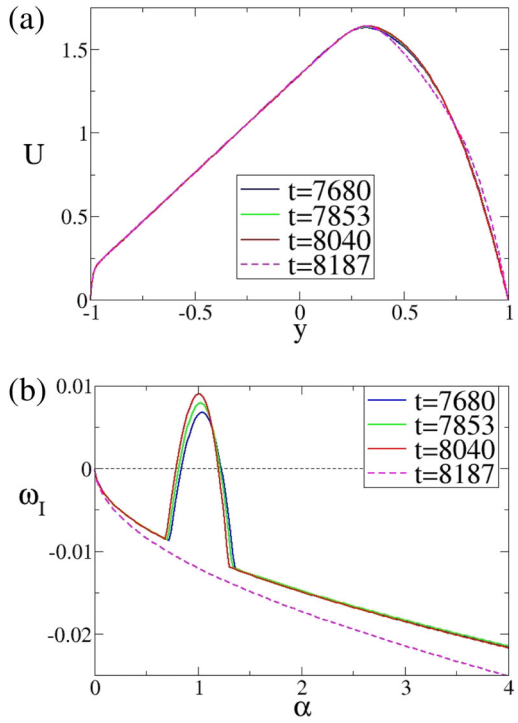


FIG. 4 (color online). (a) Mean velocity profiles (WTS corresponds to $y \gtrsim 0.25$) and (b) growth rates (imaginary part of $\omega$) versus $\alpha$ of $\beta = 0$ modes at different times.

grows by 2 orders of magnitude. The wave amplitude needs 307 time units to grow by one decade, which explains the long intervals between bursts. Variations in the bursting period are due to the stochastic nature of the background fluctuations. The eigenfunction [Fig. 5(b)] and frequency obtained from linear analysis also match simulation results, proving that a linear instability with a large amplitude on the WTS produces the exponentially growing plane wave in RPF and is the principal driving mechanism for the cyclic bursts. This process is self-sustained since, besides the driving pressure gradient, no external trigger is needed to maintain it. In the simulation the pressure force was varied to keep the mass flow rate constant, but a constant pressure force produces essentially the same cyclic bursts.

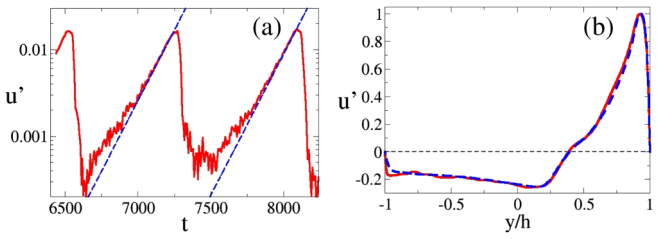


FIG. 5 (color online). (a) Amplitude $u'$ and (b) profile at $t = 8040$ of the $(\alpha = 1, \beta = 0)$ mode in the simulation (red lines) compared to the growth rate and eigenfunction predicted by the linear stability analysis (blue dashed lines).

We may speculate on what happens in currently out-of-reach simulations with extended domains. The linear instability would still occur in such domains, but the competition between different wavelengths and phases could lead to nonuniform or even localized bursts and hence spatiotemporal intermittency.

RPF simulations to be reported in a forthcoming study, mapping out an extensive parameter range, demonstrate that cyclic bursts also happen at higher $\Omega$ and higher or lower $R$ until a critical $R_c = 3848$ when TS waves become stable in Poiseuille flow according to linear theory. However, at higher $\Omega$ and lower $R$ turbulence is less intense and RPF can even partly or completely relaminarize [12]; instabilities in a turbulent environment are thus merely found at higher $R$. Relaminarization and extreme amplitude states at low $R$ have recently been studied [17].

Other external forces or conditions can also alter turbulence and mean velocity profiles, suggesting that instabilities can happen in other hydrodynamical systems. Cyclic bursts of turbulence caused by a linearly unstable TS wave have indeed been observed in low magnetic Reynolds number Poiseuille flow with a steady spanwise magnetic field at $R = 5333$ [18,19]. Between the bursts, the flow is fully laminar since the Lorentz force suppressed turbulence. Our study shows that the absence of turbulence is not a prerequisite for a linear instability. Indeed, we conducted magnetic simulations at $R = 20000$, where the flow does not fully relaminarize, and identified cyclic bursts for strong magnetic fields similar to RPF. Unlike in [18], no noise is needed to sustain the cycle since the flow is always subject to turbulent fluctuations. A difference to RPF is the statistical symmetry of the magnetic case about the center line.

To summarize, rotation changes the flow in strongly turbulent RPF in such a way that it becomes receptive to a linear instability, despite the strong turbulence, and a simple reduced model can describe this driving instability. The turbulence results from deterministic dynamics as opposed to parametrizable external noise, and has a wide range of temporal and spatial scales. We are able to describe and understand all phases leading to the recurrent intense low-frequency bursts. This case strongly suggests a low-dimensional dynamic system embedded in an environment with strong fluctuations. Low-dimensional bursting dynamics are also found in accretion disks [20] and tokamaks [21], where the full interaction between large-scale modes and small-scale fluctuations deserves further study. The present study offers some important insights; environments with inhomogeneous strong fluctuations can support cyclic instabilities of a large-scale mode. The simple and well-defined RPF with its multifaceted physics is a valuable alternative to other flows featuring shear and rotation such as Taylor-Couette and von Kármán flows.

We acknowledge PRACE for awarding us via the REFIT project access to the resource Jugene at the Jülich Supercomputing Centre in Germany. Computational resources at PDC were made available by SNIC. We thank Liang Wei for producing some of the visualizations. The project was supported by the Swedish Research Council through Grants No. 621-2010-4147 and No. 621-2013-5784.

*geert@mech.kth.se

[1] P. L. McFadden, R. T. Merrill, M. W. McElhinny, and S. Lee, J. Geophys. Res. **96**, 3923 (1991).
[2] J. Imbrie *et al.*, Paleoceanography **7**, 701 (1992); M. Collins *et al.*, Nat. Geosci. **3**, 391 (2010); K. Stein, A. Timmermann, and N. Schneider, Phys. Rev. Lett. **107**, 128501 (2011).
[3] R. T. J. McAteer, P. T. Gallagher, and P. A. Conlon, Adv. Space Res. **45**, 1067 (2010).
[4] H.-D. Xi, S.-Q. Zhou, Q. Zhou, T.-S. Chan, and K.-Q. Xia, Phys. Rev. Lett. **102**, 044503 (2009); K. Sugiyama, R. Ni, R. J. A. M. Stevens, T. S. Chan, S.-Q. Zhou, H.-D. Xi, C. Sun, S. Grossmann, K.-Q. Xia, and D. Lohse, Phys. Rev. Lett. **105**, 034503 (2010);S. Weiss and G. Ahlers, J. Fluid Mech. **676**, 5 (2011).
[5] F. Ravelet, L. Marié, A. Chiffaudel, and F. Daviaud, Phys. Rev. Lett. **93**, 164501 (2004); A. de la Torre and J. Burguete, Phys. Rev. Lett. **99**, 054101 (2007); E. Herbert, P.-P. Cortet, F. Daviaud, and B. Dubrulle, Phys. Fluids **26**, 015103 (2014).
[6] A. Gailitis, O. Lielausis, E. Platacis, S. Dement'ev, A. Cifersons, G. Gerbeth, T. Gundrum, F. Stefani, M. Christen, and G. Will, Phys. Rev. Lett. **86**, 3024 (2001); F. Ravelet *et al.*, Phys. Rev. Lett. **101**, 074502 (2008); M. Berhanu *et al.*, J. Fluid Mech. **641**, 217 (2009); R. Monchaux *et al.*, Phys. Fluids **21**, 035108 (2009).
[7] P. Beyer, S. Benkadda, G. Fuhr-Chaudier, X. Garbet, P. Ghendrih, and Y. Sarazin, Phys. Rev. Lett. **94**, 105001 (2005);M. Leconte, P. Beyer, X. Garbet, and S. Benkadda, Phys. Rev. Lett. **102**, 045006 (2009).
[8] E. I. Vorobyov and S. Basu, Astrophys. J. **719**, 1896 (2010); R. G. Martin, S. H. Lubow, M. Livio, and J. E. Pringle, Mon. Not. R. Astron. Soc. **420**, 3139 (2012); D. Stamatellos, A. P. Whitworth, and D. A. Hubber, Mon. Not. R. Astron. Soc. **427**, 1182 (2012); J. Bae, L. Hartmann, Z. Zhu, and C. Gammie, Astrophys. J. **764**, 141 (2013).
[9] H. J. Brauckmann and B. Eckhardt, Phys. Rev. E **87**, 033004 (2013); D. P. M. van Gils, S. G. Huisman, S. Grossmann, C. Sun, and D. Lohse, J. Fluid Mech. **706**, 118 (2012).
[10] D. J. Tritton, *Physical Fluid Dynamics* (Oxford University Press, New York, 1988).
[11] M. Chevalier, P. Schlatter, A. Lundbladh, and D. S. Henningson, KTH Mechanics Report No. TRITA-MEK 2007:07, 2007.
[12] R. Kristoffersen and H. I. Andersson, J. Fluid Mech. **256**, 163 (1993); O. Grundestam, S. Wallin, and A. V. Johansson, J. Fluid Mech. **598**, 177 (2008).
[13] A. Prigent, G. Grégoire, H. Chaté, O. Dauchot and W. van Saarloos, Phys. Rev. Lett. **89**, 014501 (2002); L. S. Tuckerman and D. Barkley, Phys. Fluids **23**, 041301 (2011); M. J. Burin and C. J. Czarnocki, J. Fluid Mech. **709**, 106 (2012).
[14] G. Brethouwer, Y. Duguet and P. Schlatter, J. Fluid Mech. **704**, 137 (2012).
[15] T. Herbert, Annu. Rev. Fluid Mech. **20**, 487 (1988).

[16] J. C. del Álamo and J. Jiménez, J. Fluid Mech. **559**, 205 (2006).
[17] S. Wallin, O. Grundestam, and A. V. Johansson, J. Fluid Mech. **730**, 193 (2013).
[18] T. Boeck, D. Krasnov, A. Thess, and O. Zikanov, Phys. Rev. Lett. **101**, 244501 (2008).
[19] P. K. Dey and O. Zikanov, Phys. Fluids **24**, 084104 (2012).
[20] S. A. Balbus and J. F. Hawley, Rev. Mod. Phys. **70**, 1 (1998); M. Tagger, P. Varniere, J. Rodriguez, and R. Pellat, Astrophys. J. **607**, 410 (2004); C. R. D'Angelo and H. C. Spruit, Mon. Not. R. Astron. Soc. **406**, 1208 (2010).
[21] A. Strugarek *et al.*, Phys. Rev. Lett. **111**, 145001 (2013).